Vol. 17, No. 3 (2018) 913-925
Revista Mexicana de Ingeniería Química

ENHANCED CATALYTIC ACTIVITY ON THE NAPHTHALENE HYDROGENATION REACTION OVER Pt-Pd/Al_2O_3-CeO_2 CATALYSTS

ACTIVIDAD CATALÍTICA MEJORADA EN LA REACCIÓN DE HIDROGENACIÓN DE NAFTALENO SOBRE CATALIZADORES DE Pt-Pd / Al_2O_3-CeO_2

M.E. Manríquez[1], M.L. Hernández-Pichardo[1]*, M.C. Barrera[3], R. Ramírez-López[1], L.V. Castro[2]

[1] *Instituto Politécnico Nacional-Escuela Superior de Ingeniería Química e Industrias Extractivas, Laboratorio de Investigación de Fisicoquímica y Materiales, UPALM, 07738, México City, México.*

[2] *Instituto Politécnico Nacional-Escuela Superior de Ingeniería Química e Industrias Extractivas, Laboratorio de Nanomateriales Sustentables, UPALM, 07738, México City, México.*

[3] *Facultad de Ciencias Químicas-Centro de Investigación en Recursos Energéticos y Sustentables, Universidad Veracruzana, Campus Coatzacoalcos, Av. Universidad km. 7.5, Col. Santa Isabel, Coatzacoalcos, Veracruz, 96538, México.*

Received November 27, 2018; February 24, 2018

Abstract

Alumina (Al_2O_3) and Alumina-Ceria (Al_2O_3-CeO_2) supports with different CeO_2 loadings (0, 2, 5, 10 and 50 wt.%) were prepared by the sol-gel method and impregnated with 0.5% of Pt and 0.5 % of Pd (wt.%). The catalysts were characterized by X-ray diffraction (XRD), Raman spectroscopy, UV-Vis diffuse reflectance spectroscopy (DRS), and scanning electron microscopy (SEM). The present work aims to study the influence of the ceria content over the catalytic activity of Pt-Pd/Al_2O_3-CeO_2 samples during the naphthalene hydrogenation reaction. The results show that as the cerium oxide content increases, the intensity of the diffraction peaks corresponding to this oxide also increases due to the high crystallinity of the ceria as compared to the polycrystalline alumina. At low CeO_2 contents, a shift of the peaks towards lower angles is observed, suggesting an incorporation of Al_2O_3 into the CeO_2 lattice. Similarly, Raman analyzes show a single band around 440 cm^{-1} attributed to the formation of ceria, whose characteristic peak has been observed at approximately 459 cm^{-1}. This shift towards smaller energies is another indication of the incorporation of alumina in the ceria lattice. Finally, the aggregation of the ceria in the support also results in a decrease in the BET area of these materials. This enhancement in the catalytic performance was related to a supplementary contribution from naphthalene adsorbed on acidic sites on the support and reacting with hydrogen migrating from platinum and palladium surface by a *spillover* effect. The activity in the naphthalene hydrogenation showed a significant influence on the interaction between the metals (Pt, Pd) and the support (Al_2O_3-CeO_2).

Keywords: naphthalene hydrogenation, Al_2O_3-CeO_2 supports, metal-support interactions, acid sites.

Resumen

Se prepararon soportes de alúmina (Al_2O_3) y alúmina-ceria (Al_2O_3-CeO_2) con diferentes contenidos de CeO_2 (2, 5, 10 y 50 en % wt) mediante el método sol-gel y se impregnaron con 0.5% de Pt y 0.5% de Pd (% wt). Los catalizadores se caracterizaron por difracción de rayos X (XRD), espectroscopía Raman, espectroscopía de reflexión difusa UV-Vis (DRS) y microscopía electrónica de barrido (SEM). El presente trabajo tiene como objetivo estudiar la influencia del contenido de ceria sobre la actividad catalítica de muestras de Pt-Pd/Al_2O_3 dopadas con este óxido, en la reacción de hidrogenación de naftaleno. Los resultados muestran que a medida que el contenido de óxido de cerio aumenta, también aumenta la intensidad de los picos de difracción correspondientes a este óxido, debido a la alta cristalinidad de la ceria comparada con la alúmina policristalina. A bajos contenidos de CeO_2, se observa un corrimiento de los picos hacia ángulos más bajos, lo que sugiere una incorporación de la Al_2O_3 en la red de la CeO_2. Asimismo, los análisis de Raman muestran una sola banda alrededor de 440 cm^{-1} atribuible a la formación de la ceria, cuyo pico característico se ha observado en aproximadamente 459 cm^{-1}. Este desplazamiento hacia energías más pequeñas es otro indicativo de la incorporación de la alúmina en la red de la ceria. Finalmente la agregación de la ceria en el soporte resulta también en un decremento del área BET de estos materiales. También se observó que la actividad catalítica aumenta con el contenido de CeO_2 en el catalizador, lo cual se relacionó con una contribución suplementaria de la adsorción de naftaleno en sitios ácidos sobre el soporte y la reacción con hidrógeno que migra desde la superficie de platino y paladio por un efecto *spillover*. La actividad de estos catalizadores en la hidrogenación de naftaleno mostró una influencia significativa de la interacción entre los metales (Pt, Pd) con el soporte (Al_2O_3-CeO_2).

Palabras clave: hidrogenación de naftaleno, soportes de Al_2O_3-CeO_2, interacciones metal-soporte, sitios ácidos.

* *Corresponding author. E-mail*: mhernandezp@ipn.mx

doi: 10.24275/uam/izt/dcbi/revmexingquim/2018v17n3/Manriquez
issn-e: 2395-8472

1 Introduction

Distillate fuels typically contain paraffins, naphthenes, and aromatics. For fuels quality parameters, such as cetane number, paraffins are the most desirable components, while the unfavorable components are multi-ring aromatic compounds due to environmental regulations. The catalytic hydrogenation reactions have been therefore the focus of many recent studies due to the interest for deep hydrogenation (HYD) of aromatics (Chen *et al*., 2015; Ju *et al*., 2015; Téllez-Romero *et al*., 2015; Escobar *et al*., 2017; Sánchez-Minero *et al*., 2010; and Liu *et al*., 2016). In particular, the hydrogenation of naphthalenes produces tetralins while the complete saturation leads to the formation of decalins. Moreover, this reaction is also of industrial interest, not only due to its role in upgrading coal liquids and diesel fuels, but also because of the production of solvents, such as tetralin (Chen *et al*., 2015).

Some other types of catalysts have been tried, with the aim of increasing the electron defficiency of noble metals via interaction with an acidic support or introducing a secondary metal (Ju *et al*., 2015). According to Chun-Mei *et al*. (2000), the hydrogenation activity of supported metal catalysts is determined by the presence of the metallic sites for the dissociated adsorption of hydrogen and the support for the adsorption of the aromatic reactants. The acidic nature of the support has been shown to play an important role for naphthalene hydrogenation reactions. Supported metallic catalysts on acidic solids such as Au-Pd/SiO_2-Al_2O_3, Pt/TiO_2-ZrO_2 or Pt/KA zeolite, have been found to enhance aromatics hydrogenation rates, superior than the conventional Co-Mo and Ni-Mo sulfide catalysts (Ju *et al*., 2015; Lu *et al*., 2000; Venezia *et al*., 2004).

Noble metal catalysts supported on ceria are particularly important due to their acid-base and redox properties of ceria (Damyanova *et al*., 2003). However, although there is an agreement in the mechanism of the hydrogenation of naphthalene, a better understanding of the effect of the support on the catalytic behavior is needed. In this work, the catalytic behavior of the bimetallic system Pt-Pd/Al_2O_3-CeO_2 was investigated pursuing the combination of the large surface area and stability of Al_2O_3 with the oxygen storage and release capability of CeO_2 at different concentrations in the hydrogenation of naphthalene reaction.

2 Experimental

2.1 Catalysts preparation

Alumina (Al_2O_3) and Alumina-Ceria (Al_2O_3-CeO_2) supports with different concentrations were prepared by sol-gel method by adding an aqueous solution of cerium nitrate to aluminum-tri-sec-butoxide in order to obtain samples with different ceria loading (0, 2, 5, 10 and 50 % wt., theoretical values). The pH value was adjusted at pH=3 in all the samples using HNO_3 and the samples were prepared using an alkoxide/ethanol ratio of 1/4. The solution of the metal alkoxide was prepared in the reactor from a dilution of aluminum-tri-sec-butoxide in isopropyl alcohol at 5°C. Once the solutions were prepared, the cerium solution and the HNO_3 were added dropwise to the alkoxide solution, which remained at 5°C with vigorous agitation throughout the time of the addition. Stirring continued for some more minutes, until the formation of the gel.

After the gelation of supports was completed, calcinations were carried out at 600 °C under oxygen flow. The supports were impregnated with aqueous solutions of platinum and palladium nitrates in order to obtain 0.2 wt % of metal in the catalyst (0.1 wt % each one). The reference catalyst Pt-Pd/Al_2O_3 and the samples synthesized with ceria (Pt-Pd/Al_2O_3-CeO_2) were identified to as PPA and PPACx respectively; where “PP" stands for those samples impregnated with Pt and Pd, whereas “A" and “C" represent alumina or ceria, respectively; finally, x denotes the nominal ceria loading (0, 2, 5, 10, 15 and 50 wt. %).

2.2 Catalysts characterization

X-Ray diffraction patterns were obtained in a Siemens D-5000 diffractometer using Cu-Ka radiation. For Raman spectroscopy studies, a MicroRaman, Jobin Yvon-Horiba Labram 800 was used. UV-Vis was determined by using a Cary 100 spectrophotometer with integration sphere along with MgO as 100% reflectance patron. The scanning electron microscopy (SEM) analyses were performed using a Quanta 3D FEG microscope and the elemental composition and mapping were obtained from Energy dispersive X-ray spectroscopy (EDS) with a spectrometer fitted to the SEM. The textural properties were determined from the nitrogen adsorption isotherms obtained with a Micromeritics ASAP 2000 automated apparatus. The specific surface areas were calculated from the

isotherms using the BET method. The surface area was calculated by the BET equation and the pore size distribution was calculated based on the method developed by Barrett, Joyner and Halenda (BJH method) using the desorption branch of the isotherm. All samples were degassed at 300 °C for 6 h before analysis.

For the FTIR-pyridine adsorption, transparent pellets of the oxides were placed in a stainless-steel sample holder with CaF_2 windows, which allows vacuum in situ and thermal treatments. The samples were desorbed at 400°C during 2 h, and then cooled down at room temperature. Thereafter, a closed capillary containing pyridine was introduced into the cell, and after the heat treatment, the capillary was broken up to allow the pyridine to be adsorbed in the sample. The pyridine was maintained in contact with the sample for 30 min. The excess of pyridine was eliminated at vacuum and pyridine desorption was accomplished by heating up from room temperature to 400 °C. The resulting spectra were obtained with a 710SX Nicolet FTIR spectrometer.

2.3 *Catalytic test*

The evaluation of the catalytic activity in the naphthalene conversion was carried out in a stirred batch reactor (Parr 4842, 450 ml vessel volume) operating at 290 °C, 5.5 MPa and 1200 rpm (~126 rad s^{-1}) mixing speed. According to the literature, this speed guarantees a fast-enough supply of reactant molecules to the catalyst particles surface in order to discard reaction control by external reactants diffusion (Escobar *et al*., 2017). The reaction mixture contained 0.2 g of catalyst (materials *ex-situ* reduced at 350 °C under H_2 flow, 60 mL min^{-1}, 1 h) and 0.3 g of naphthalene dissolved in 100 mL of hexadecane. All reagents were supplied by Sigma-Aldrich. Catalytic runs typically lasted 2 h. Reaction products were analyzed by GC (Agilent Technologies 6890N) equipped with a flame ionization detector and a capillary column (5% phenyl-95% methylpolysiloxane, Econo-Cap-5, from Alltech). From previous experiments reported in the literature the appropriate conditions were determine to avoid reaction control by either interfacial or intra-particle diffusion (particle size ~165 μm) (Escobar *et al*., 2017). The results of naphthalene hydrogenation were also compared with the Pt-Pd/Al_2O_3 reference catalyst.

3 Results and discussion

3.1 *Textural properties*

Five different Pt-Pd/Al_2O_3-CeO_2 bimetallic catalysts at different ceria contents were studied. The chemical compositions, textural properties (surface area, pore volume and main pore size) and CeO_2 crystallite size of the different samples are shown in Table 1. The main pore size values were determined by the BJH method using the main value of the monomodal pore size distribution (not shown). From the textural results depicted in Table 1, it is observed that the reference catalyst Pt-Pd/Al_2O_3 (PPA) and the samples with a lower content of ceria (PPAC2 and PPAC5), showed the highest values of surface area and pore size. The highest values were obtained for the sample with 2% of CeO_2 (PPAC2), with a maximum of 359 m^2 g^{-1} and 1.16 cm^3 g^{-1}. These values are consistent with those reported in literature for samples prepared by the sol-gel method (Luisetto *et al*., 2015; Liotta *et al*., 2003). It was also observed that the addition of higher quantities of ceria (10 and 50% wt.) decreases the values of the average pore diameter, the surface areas and the pore volumes, due to the presence of higher content of ceria, which exhibits a smaller surface area. The specific area is probably affected by some Ce^{3+} cations occupying vacant octahedral coordinated sites on the surface of alumina. At the same time, the occupation of the octahedral sites by cerium cations may block the transition of Al^{3+} cations from tetrahedral to octahedral, which is partially, the cause of the loss of surface area in the materials (Yuan *et al*., 2009). Moreover, the aggregation of the ceria in the support results in a decrease in the BET area of these materials. From the SEM images showed in Figure 1, few differences can be observed for the Pt-Pd/Al_2O_3-CeO_2 catalysts. The materials have a heterogeneous form, forming dense aggregates, the porosity in these samples may be due partially by interparticle space. EDS analyzes were performed in order to see the presence of the elements and percentage of elemental composition on the surface of all the samples. As an example, the EDS spectrum for the PPAC50 sample is shown in Fig. 1e. From these results, it was found out that the concentrations were very similar to the nominal contents.

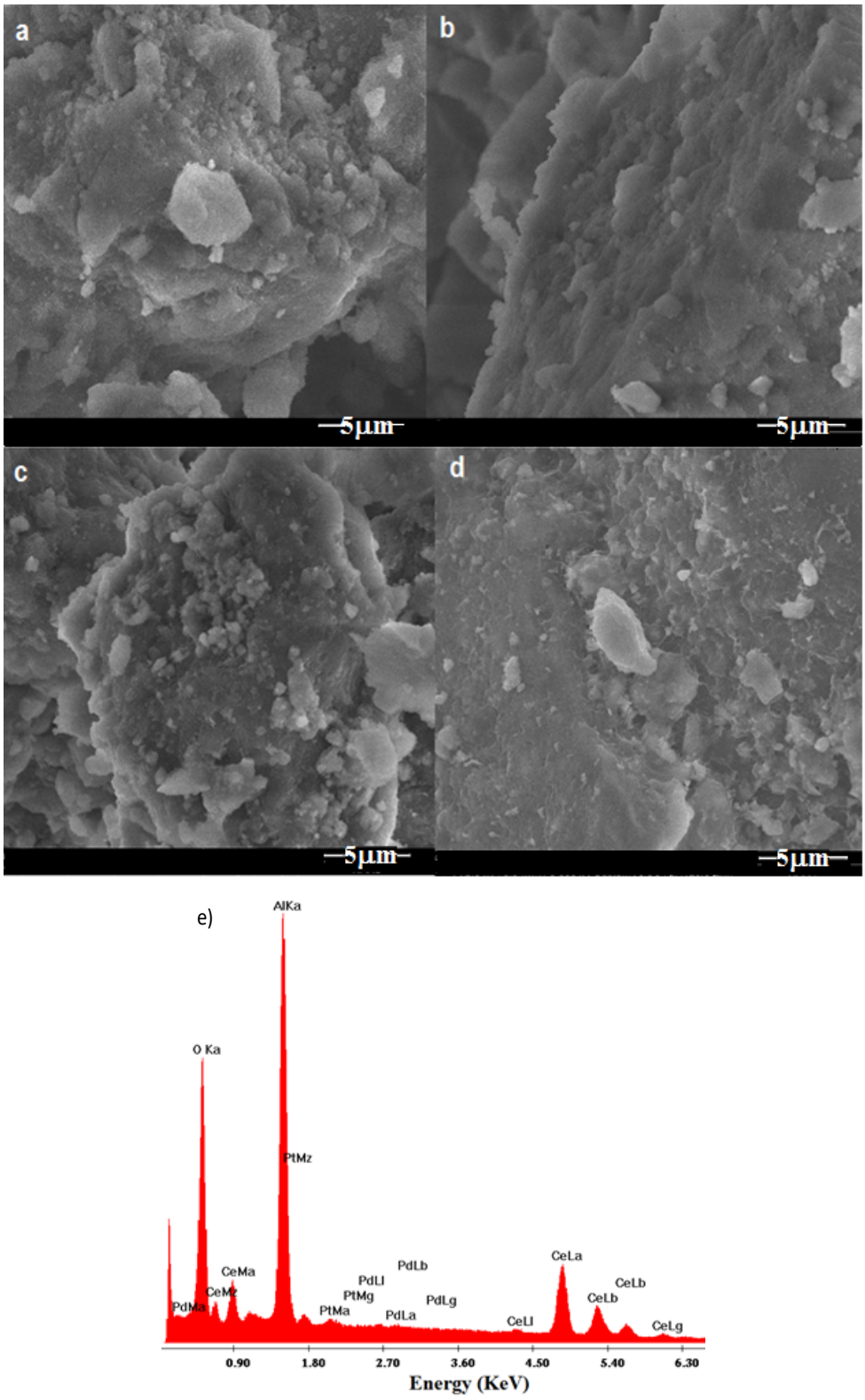

Fig. 1. Typical SEM images of samples: a) PPA, b) PPAC2, c) PPAC10, d) PPAC50, and, e) EDS analysis for the PPAC50 sample.

Table 1. Compositions, textural properties and CeO_2 crystallite size of the Pt-Pd/Al_2O_3 and Pt-Pd/Al_2O_3-CeO_2 catalysts.

Catalyst	CeO_2 (wt.%)	Al_2O_3 (wt.%)	Pt (wt.%)	Pd (wt.%)	SBET ($m^2\ g^{-1}$)	Pore volume ($cm^3\ g^{-1}$)	Pore diameter (Å)	$d^*_{CeO_2}$ (nm)
PPA	0	100	0.1	0.1	326	0.87	107	–
PPAC2	2	98	0.1	0.1	359	1.16	129	6.3
PPAC5	5	95	0.1	0.1	318	1.03	120	5.7
PPAC10	10	90	0.1	0.1	208	0.66	99	4.4
PPAC50	50	50	0.1	0.1	85	0.12	59	3.2

*Calculated from XRD by Scherrer's equation.

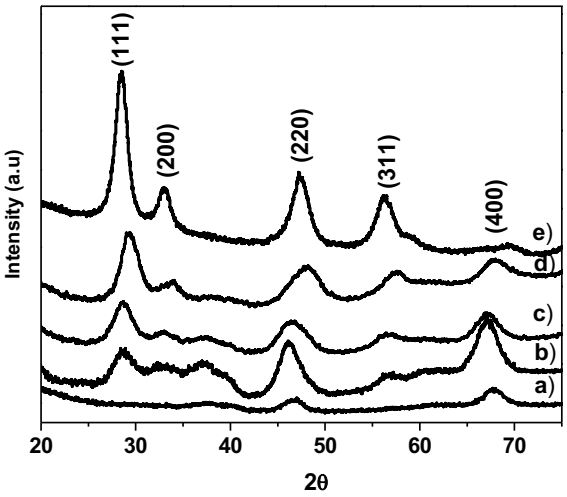

Fig. 2. X-ray powder diffraction patterns of the prepared catalysts a) PPA, b) PPAC2, c) PPAC5, d) PPAC10, and e) PPAC50.

3.2 Structural properties

Figure 2 shows the XRD patterns of the Pt-Pd/Al_2O_3-CeO_2 catalysts. The patterns of the catalysts prepared with ceria show diffraction peaks at 2θ = 28.6°, 33.1°, 47.5°, 56.3° and 69.5° assigned to the crystalline planes (111), (200), (220), (311) and (400) of CeO_2 cubic phase, (PDF 65-5923), and Al_2O_3 (2θ = 37.6°, 45.8°, 66.7°) (PDF 02-1420), indicating that the samples are polycrystalline. The increase in ceria content results in a progressive crystallization of CeO_2. All of the ceria peaks can be indexed as a pure cubic phase (space group: *Fm3m* (225)) of a cubic fluorite structure of CeO_2 (Torrente-Murciano *et al*., 2013). These patterns show broad peaks, which confirmed the formation of small nanoparticles. The ceria crystallite sizes, obtained from the Scherrer equation using X-ray line broadening of the (111) peak, ranged from 3.2 to about 6.3 nm (see Table 1), thus decreasing with the ceria content. The analysis of the line broadening at half the maximum intensity (FWHM) indicated that this peak becomes narrow as the ceria content increases, which is an indication of the reduction of the size of crystallite. In the Al_2O_3-CeO_2 systems, it has been found out that both CeO_2 and Al_2O_3 delayed the crystalline phase transformations for each other (Bose *et al*., 1999), hence avoiding the growth of the particle size.

The diffraction patterns also reveal a preferential growth along the direction (111) imposed by the synthesis conditions. It is well-known that CeO_2 holds the fluorite structure, in which the low-index (111) surface has the lowest surface energy and is thus the most stable surface, and consequently the one which is predominantly exposed (Mai *et al*., 2005; Sayle *et al*., 2002). The preferential growth in a crystallographic orientation is determined by the synthesis method or the interaction with other species present in the synthesis (Sayle *et al*., 2002; Tsivion *et al*., 2012). In this case, the preferential growth along the direction (111) is due to their epitaxial relation with the Al_2O_3 surface, as well as by a graphoepitaxial effect that guides their growth along surface steps and grooves (Melchionna *et al*., 2014; Tsivion *et al*., 2012). Moreover, a theoretical study (Sayle *et al*., 2002) suggested that CeO_2 supported on Al_2O_3, exhibits a lower oxygen formation energy as compared with the unsupported CeO_2. Therefore, the preferential growth along this direction could indicate that the oxidizing power of the ceria is decreasing, thus increasing the surface acidic properties.

The Raman spectra of the Pt-Pd/Al_2O_3-CeO_2 samples are shown in Figure 3. It is observed that, in agreement with other observations in the literature, the Raman spectrum of Al_2O_3 calcined at 600 °C does not contain any signal, being very similar to the spectrum

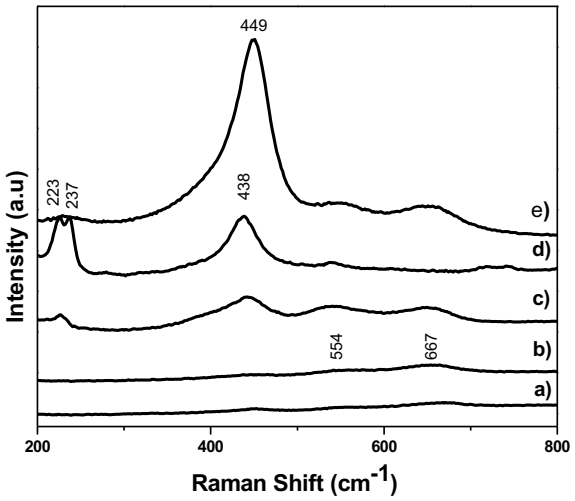

Fig. 3. Raman spectra of the Pt-Pd/Al_2O_3-CeO_2 catalysts calcined at 600 °C: a) PPA, b) PPAC2, c) PPAC5, d) PPAC10, and e) PPAC50.

of the sample with 2% of CeO_2 (PPAC2). Although it is possible that the small bands at about 554 and 667 cm^{-1} in these spectra may be attributed to the Pt-O stretching vibrations associated with adsorbed water (Brogan and Raman, 2000). It is also observed that as the amount of ceria is increased, the materials transform from the tetragonal phase and tend to form the fluorite-structured CeO_2 phase with a main band located at about 450 cm^{-1} and another less intense band at 550 cm^{-1} (Jiang M. *et al*., 2013). The first band around 440 cm^{-1} corresponds to the Raman-active F_{2g} mode and represents a symmetrical stretching of the Ce-O vibration in the fluorite structure, while the second one appears due to the presence of extrinsic oxygen vacancies in ceria when it is mixed or doped with other metals (Du *et al*., 2017; Cho, 1991). The F_{2g} band gradually shifts towards a higher wavenumber as the ceria content increases suggesting that CeO_2 has diffused into the Al_2O_3 lattice. The band at about 649 cm^{-1} in the Pt-Pd/Al_2O_3-CeO_2 samples has been attributed to defects and oxygen displacements that distort the cubic structure. Finally, within region 223 to 237 cm^{-1}, the peaks are assigned to Pt-O and Pd-O bonds. These results, along with XRD analysis, confirm the formation of Al_2O_3-CeO_2 mixed oxides.

The UV-vis spectra were obtained in order to identify the different chemical species in the Pt-Pd/Al_2O_3-CeO_2 system (Figure 4) over the region UV between 200 and 300 nm. The spectrum of Pt-Pd/Al_2O_3 sample (Figure 4e) shows a broad band at about 240 nm, which can be assigned to metals-oxygen charge transfer (Feio *et al*., 2007).

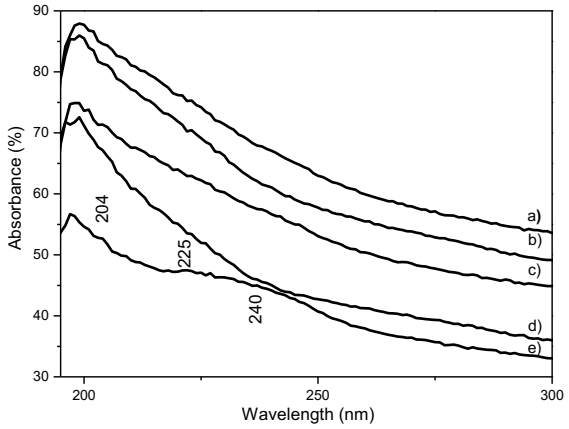

Fig. 4. UV-Vis diffuse reflectance spectra of Pt-Pd/Al_2O_3-CeO_2 samples with different CeO_2 contents: a) PPAC50, b) PPAC10 c) PPAC5, d) PPAC2 and e) PPA.

This band became hardly visible for the ceria containing samples, even at low loadings, probalby due to the absorption bands from several transitions assigned to the cerium species. The presence of the absorption bands between 200 to 250 nm may occur because of the 4f-5d transitions from isolated Ce^{3+} ions on the surface or in the alumina lattice (Profeti *et al*., 2009; Ho *et al*., 2005). Also, the $O_2 \rightarrow Ce^{4+}$ charge transfer transitions may show absorption bands between 250 and 350 nm (Feio *et al*., 2007; Profeti *et al*., 2009). It has been reported that in this UV range, a band located at 272 nm may also appear, which might be assigned to the $Ce^{3+} \rightarrow Ce^{4+}$ charge transfer transition (Profeti *et al*., 2009). However, we have to consider that, in the range of 250 to 350 nm, the bands could also have contributions from electrons bonding negatively charged hydroxyls over the alumina surface and octahedral Pt species (López *et al*., 1994).

3.3 Acidic properties

Figure 5 shows the pyridine desorption as a function of temperature for the Pt-Pd/Al_2O_3 samples. In the FTIR-pyridine adsorption spectra, only Lewis acid sites can be seen in all the catalysts. The spectra show absorption bands at about 1590, 1490 and 1450 cm^{-1}, which have been assigned to pyridine adsorbed on the Lewis acid sites; while a Brönsted acidity, at 1540 and 1640 cm^{-1} was not observed in any sample. It is also found out that after rising the temperature up to 400 °C a small peak at 1450 cm^{-1} remains in almost all the catalysts, but it is more noticeable in the sample PPAC50.

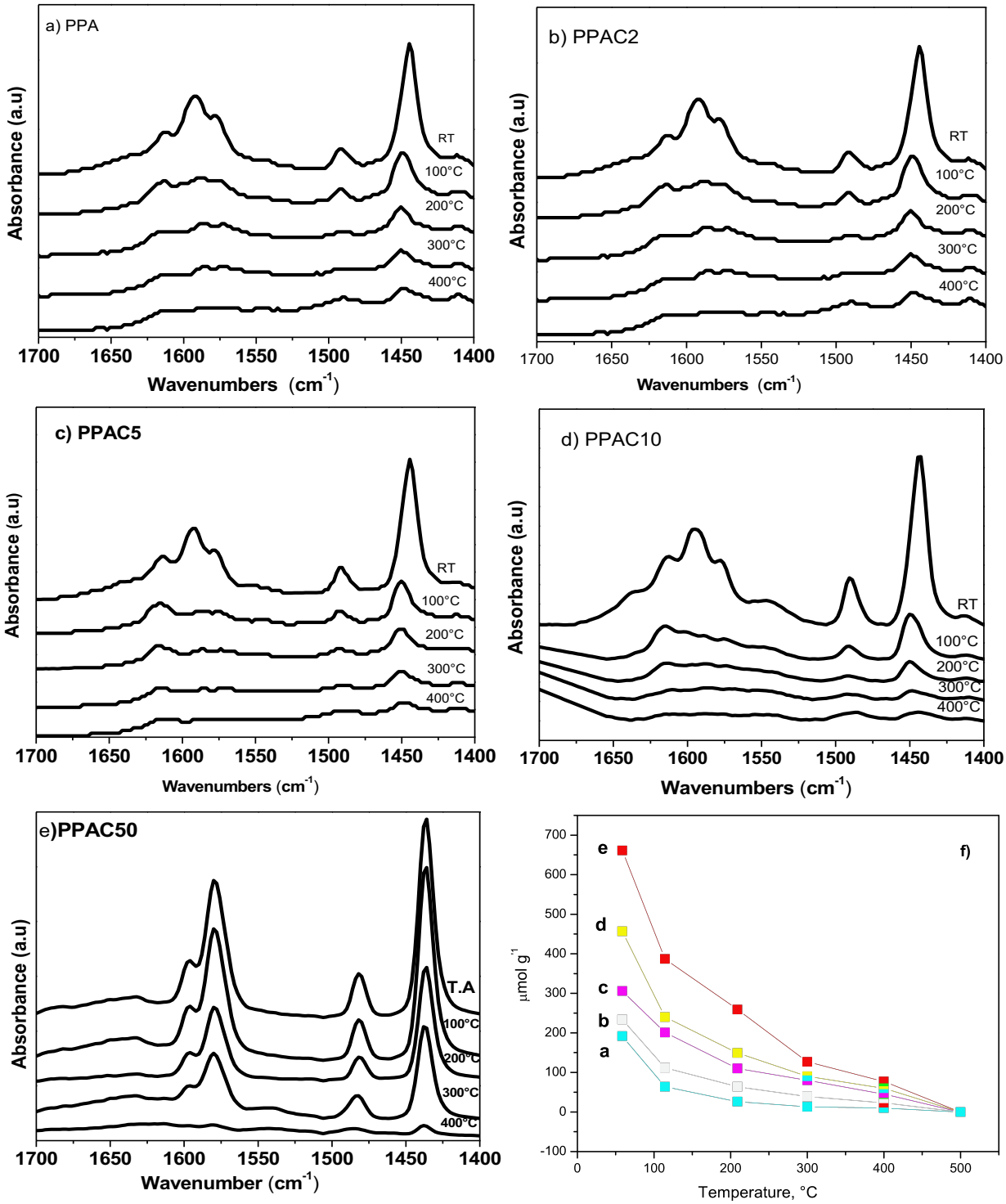

Fig. 5. FTIR spectra of adsorbed pyridine (a-e) and total acidity and amounts of Brönsted acid and Lewis acid (f) of the catalysts, thermally annealed at 400 °C.

This result suggests that the acidity increases with increase of the ceria content. These results also show that the nature of the acid sites is not modified by the presence of cerium oxide.

3.4 Catalytic test

The catalytic activity was tested for the naphthalene hydrogenation reaction at 290 °C, on Pt-Pd/Al_2O_3-CeO_2 catalysts with variations of the CeO_2 content (2, 5, 10 and 50 wt %). Figure 6 shows the concentrations versus time profiles of the naphthalene hydrogenation reaction at 290 °C, over Pt-Pd/ Al_2O_3-CeO_2 catalysts. It is observed that the naphthalene hydrogenation occurs in the two common reported steps: the conversion to tetralin, followed by the formation of decalin (Scheme 1). It was assumed that hydrogen in the reactor was in excess and constant, so the reversible reactions of hydrogenation were neglected (Huang *et al*., 1995). It is observed an increase in the rate of formation of decalin with the increase of ceria content.

The influence of the incorporation of ceria into alumina lattice on the catalytic activity are also shown in Table 2 and Figure 7. It is observed that after 30 min of reaction, the naphthalene reached a higher conversion and selectivity to tetralin on the catalysts with the higher content of ceria (PPAC50). It is well known that the metal-support interactions can be assessed with the help of probe reactions such as hydrogenation reactions. From the present results, it is clear that the activity in the hydrogenation of naphthalene shows significant influence on the interaction between the metals and the support. The activity is increasing with CeO_2 content and this increase can be correlated with the increase of the acidity of the support. The ceria-doped alumina catalysts showed higher intensity and definition of the Lewis acid sites determined by pyridine absorption spectra (Figure 5). The effect of cerium oxide in the acidity is probably due to the modification of the aluminum coordination with ions of Ce^{4+}. The acidic properties were modified due to these ions acting as Lewis acid sites.

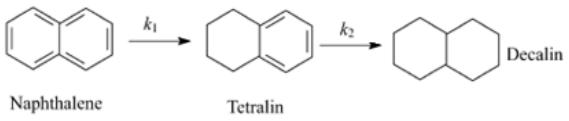

Scheme 1. Naphthalene hydrogenation reaction pathway.

According to Morterra *et al*. (1996), two pyridine bands at 1595 and 1623 cm^{-1} were ascribed to the adsorption of pyridine on Ce^{4+} centers, although pyridine is adsorbed in this region for all types of Lewis acid sites. These bands were observed in all spectra of these catalysts. In this reaction, the Lewis acid sites, act as electron-deficient centers, and the π electrons of the aromatic molecule of naphthalene tend to be electron donors. The naphthalene molecules are adsorbed on the surface of Lewis acid sites of Pt-Pd/Al_2O_3-CeO_2 to produce tetralin.

Of course, the naphthalene hydrogenation also depends on the metallic function, but since the nominal content of platinum and palladium was the same for all the catalysts, the higher performance cannot be related exclusively to the presence of Pt^0 and Pd^0 species. In addition, it is also important to note that the metallic dispersion on the supports it is not known. Moreover, some works have proposed that the interaction between metallic particles and acidic supports resulted in highly active catalysts for hydrogenation reactions (Albertazzi *et al*., 2004; Escobar *et al*., 2016). Similar results were obtained by Albertazzi *et al*. (2004), showing that the acidity of the support is a key parameter because it can hydrogenate and isomerize the ring-opening reactions and avoid side cracking reactions. The hydrogenation activity was mainly attributed to the noble metals while the selectivity was associated to both the support acidity and the Pd/Pt alloy.

Consequently, these results suggest that the increase in the catalytic activity cannot be associated merely to the textural properties or the metallic function. This enhanced catalytic activity obtained with more acidic supports is associated with an additional contribution from the naphthalene adsorbing on acidic sites of the Al_2O_3-CeO_2 supports and reacting with spilled-over hydrogen. This phenomena was also observed during the benzene hydrogenation over acidic supports (Lin, 1993). The increase in acidity is also because ceria is exposed to a reducing environment, and it can readily change the oxidation states between Ce^{3+} to Ce^{4+}, while alumina is relatively very stable. Then, the activity of the Pd-Pt/Al_2O_3 catalyst could be promoted by the addition of Ce. The metal-ceria interaction was believed to influence the electronic structure of Pt or Pd and to be responsible for the promoting effect in the catalytic activity, due to the enhancement of the redox properties of the active centers in the catalysts. The redox pair is observed by UV-vis spectroscopy in the transition of Ce^{3+}/Ce^{4+}.

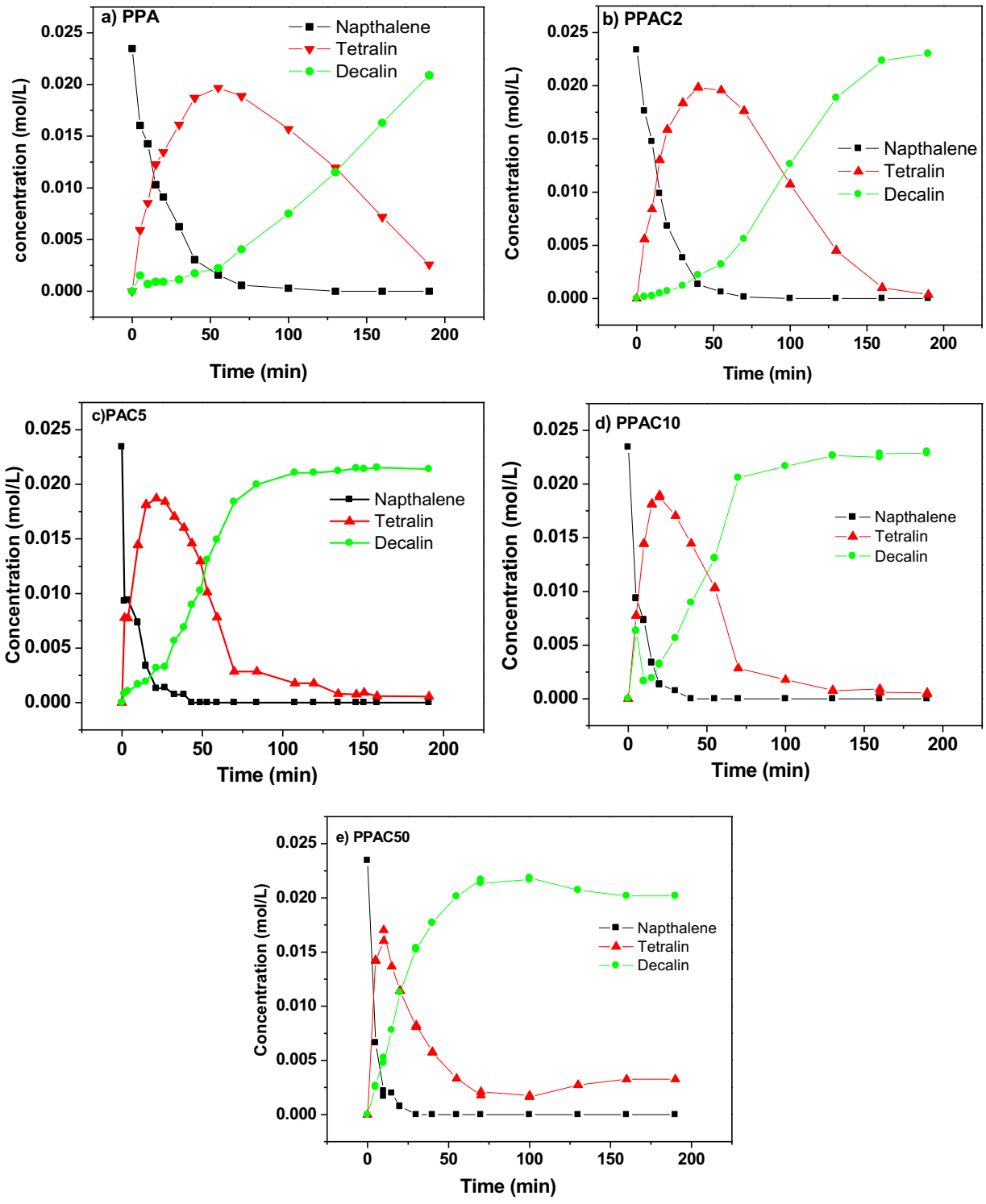

Fig. 6. Concentration vs. time profiles of naphthalene hydrogenation at 290 °C on Pt-Pd/ Al_2O_3-CeO_2 catalysts: a) PPA, b) PPAC2, c) PPAC5, d) PPAC10 and e) PPAC50.

Table 2. Naphthalene conversion and selectivity of the Pt-Pd/Al_2O_3-CeO_2 catalysts.

Catalyst	X_A (% mol)	Selectivity (% mol)	
		Tetralin	Decalin
PPA	0.861	0.618	0.382
PPAC2	0.907	0.738	0.252
PPAC5	0.945	0.756	0.244
PPAC10	0.972	0.764	0.236
PPAC50	0.995	0.805	0.195

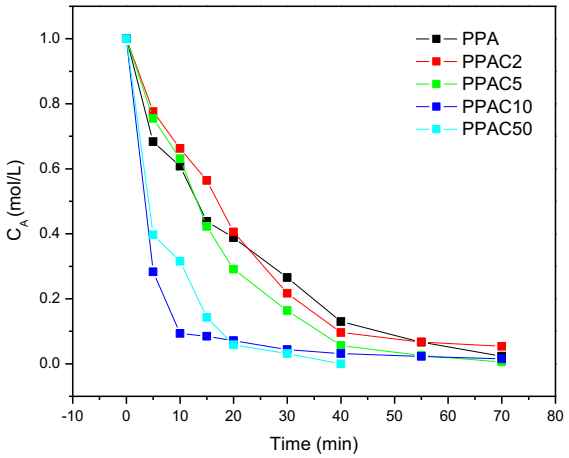

Fig. 7. Comparison of concentration vs. time profiles, naphthalene hydrogenation at 290 °C.

In summary, it is well-known that hydrogenation reactions are favored by the use of metallic catalysts with high hydrogenating power such as Pt and Pd. In this work, it was found that the hydrogenation reaction of naphthalene is favored not only by the use of supported Pt-Pd bimetallic catalysts, but also by the addition of CeO_2 to the Al_2O_3 support. It was found that cerium oxide favors the hydrogenation reaction and selectivity towards tetralin. This may occur because there is a strong attraction between CeO_2 and Pt-Pd metals, but in a reducing atmosphere, the temperature to reduce Pt or Pd to the metallic state decreases while CeO_2 remains unchanged, as reported by some authors (Wenyong *et al.*, 2008). This fact favors the hydrogenation reaction. Likewise, when CeO_2 is incorporated to the support, the acidity of the material increases, however, the acidity is not excessively strong, thus avoiding cracking reactions and favoring the selectivity towards the production of tetralin (Jiao *et al.*, 2014). The results obtained can be seen in Table 2, where it is observed that with the addition of CeO_2 the reaction is more selective to the formation of tetralin, while the production of decalin decreases. This is because the CeO_2 causes an easier reduction of both Pt and Pd, and the hydrogenation reactions are favored through the metallic function. Moreover, when CeO_2 is incorporated to the Al_2O_3 the stability and the acidity of the supports are increased, favoring the selectivity towards the production of tetralin. Furthermore, in Figures 6 and 7 it can also be seen that the maximum concentration of tetralin is obtained in less time when the amount of CeO_2 is increased. Comparatively with some reports in literature, these catalysts have higher decalin production than Pt or Pd monometallic catalysts supported on Al_2O_3 or TiO_2 (Lin and Song, 1996).

Conclusions

Ceria-doped Alumina solids were used as supports of platinum and palladium for naphthalene hydrogenation catalysts. These Pt-Pd/Al_2O_3-CeO_2 catalysts showed enhanced catalytic activity in naphthalene hydrogenation due to not only to the metallic function, but also to an additional contribution from the naphthalene adsorbing on acidic sites of the Al_2O_3-CeO_2 supports, reacting with spilled-over hydrogen. The acidity increase is due to the presence of Ce^{4+} species, which favored the activity in the hydrogenation of naphthalene. The metal-ceria interaction was believed to influence the electronic structure of the metals and to be responsible for the promoting effect in the catalytic activity, due to the enhancement of the redox properties of the active sites.

Acknowledgements

The authors would like to acknowledge to the Instituto Politécnico Nacional for the financial support received through the projects SIP- 20180761 and 20180807.

References

Albertazzi S., Rodríguez-Castellón E., Livi M., Jiménez-López A. and Vaccari A. (2004). Hydrogenation and hydrogenolysis/ring-opening of naphthalene on Pd/Pt supported on zirconium-doped mesoporous silica catalysts. *Journal of Catalysis 228*, 218-224. https://doi.org/10.1016/j.jcat.2004.07.023.

Angel G. Del, Padilla J.M., Cuauhtemoc I. and Navarrete J. (2008). Toluene combustion on Al_2O_3-CeO_2 catalysts prepared from boehmite and cerium nitrate. *Journal of Molecular Catalysis 281*, 173-178. https://doi.org/10.1016/j.molcata.2007.08.017.

Bose S. and Wu Y. (2005). Synthesis of Al_2O_3-CeO_2 mixed oxide nano-powders. *Journal of the American Ceramic Society 88*, 1999-2002. https://doi.org/10.1111/j.1551-2916.2005.00378.x.

Brogan M.S., Dines, T.J. and Cairns J.A. (1994) Raman Spectroscopic Study of the Pt-CeO, Interaction in the Pt/Al_2O_3-CeO Catalyst. *Journal of the Chemical Society Faraday Transactions 90*, 1461-1466. http://dx.doi.org/10.1039/FT9949001461.

Chen, X., Ma Y., Wang L., Yang Z., Jin S. and Zhang L. (2015). Nickel-aluminum intermetallic compounds as highly selective and stable catalysts for the hydrogenation of naphthalene to tetralin. *Chem Cat Chem 7*, 978-983. https://doi.org/10.1002/cctc.201402957.

Cooper B.H. and Donnis B.B.L. (1996). Aromatic saturation of distillates: an overview. *Applied Catalysis A 137*, 203-223. https://doi.org/10.1016/0926-860X(95)00258-8.

Cho, B. K. (1991). Chemical modification of catalyst support for enhancement of transient catalytic activity: nitric oxide reduction by carbon monoxide over rhodium. *Journal of Catalysis 131*, 74-87. https://doi.org/10.1016/0021-9517(91)90324-W.

Damyanova S. and Bueno J.M.C. (2003). Effect of CeO_2 loading on the surface and catalytic behaviors of CeO_2-Al_2O_3-supported Pt catalysts. *Applied Catalysis A 253*,135-150. https://doi.org/10.1016/S0926-860X(03)00500-3.

Du H., Wan T., Qu B., Scott J., Lin X. and Younis A. (2017). Tailoring the multi-functionalities of one-dimensional ceria nanostructures via oxygen vacancy modulation. *Journal of Colloid Interface Science 504*, 305-314. https://doi.org/10.1016/j.jcis.2017.05.05.

Escobar J., Núñez S., Montesinos-Castellanos A., de los Reyes J. A., Rodríguez Y. and González O. (2016). Dibenzothiophene hydrodesulfurization over PdPt/Al_2O_3-TiO_2. Influence of Ti-addition on hydrogenating properties. *Materials Chemical Physics 171*, 185-194. https://doi.org/10.1016/j.matchemphys.2016.01.004.

Escobar J., Barrera M.C., Santes V. and Terrazas J.E. (2017). Naphthalene hydrogenation over Mg-doped Pt/Al_2O_3. *Catalysis Today 296*, 197-204. https://doi.org/10.1016/j.cattod.2017.04.064.

Feio L.S.F., Hori C.E., Damyanova S., Noronha F.B. and Cassinelli W.H. (2007). The effect of ceria content on the properties of Pd/CeO_2/Al_2O_3 catalysts for steam reforming of methane *Applied Catalysis A 316*, 107-116. https://doi.org/10.1016/j.apcata.2006.09.032.

Ho Ch., Yu J., Kwong T., Mak A. C. and Lai S. (2005). Morphology-controllable synthesis of mesoporous CeO_2 nano- and microstructures. *Chemistry of Materials 17*, 4514-4522. DOI: 10.1021/cm0507967.

Huang T. and Kang B (1995). Kinetic study of naphthalene hydrogenation over Pt/Al_2O_3 catalyst. *Industrial and Engineering Chemistry Research 34*, 1140-1148. DOI: 10.1021/ie00043a016.

Jiang M., Wang B., Yao Y., Li Z., Ma X., Qin S. and Sun Q. (2013). A comparative study of CeO_2-Al_2O_3 support prepared with different methods and its application on MoO_3/CeO_2-Al_2O_3 catalyst for sulfur-resistant methanation. *Applied Surface Science 285*, 267-277. https://doi.org/10.1016/j.apsusc.2013.08.049.

Jiao Y., Wang J., Zhu Q., Li X. and Chen Y. (2014). Catalytic cracking of RP-3 jet fuel over Pt/CeO_2-Al_2O_3 by adding Cu/ZSM-5. *Energy and Fuels 28*, 5382-5388. DOI: 10.1021/ef500374c.

Ju C., Wang Y., Huang Y. and Fang Y. (2015). Design of mesoporous KA zeolite supported sulfur-tolerant noble metal catalyst for naphthalene hydrogenation. *Fuel 154*, 80-87. https://doi.org/10.1016/j.fuel.2015.03.035.

Lin, S. and Song Ch. (1996). Noble metal catalysts for low-temperature naphthalene hydrogenation in the presence of benzothiophene. *Catalysis Today 31*, 93-104. https://doi.org/10.1016/0920-5861(96)00038-7.

Lin W., Herzing A.A., Kiely C.J. and Wachs I.E. (2008). Probing metal-support interactions under oxidizing and reducing conditions: *In situ* raman and infrared spectroscopic and scanning transmission electron microscopic-X-ray energy-dispersive spectroscopic investigation of supported platinum catalysts. *Journal of Physical Chemistry C 112*, 5942-5951. DOI: 10.1021/jp710591m.

López, T., Asomoza M. and Gómez R. (1994). Spectroscopic study of Pt-Sn/Al_2O_3 sol-gel catalysts. *Materials Letters 19*, 199-206. https://doi.org/10.1016/0167-577X(94)90156-2.

Lu C., Lin Y. and Wang I. (2000). Naphthalene hydrogenation over Pt/TiO_2-ZrO_2 and the behavior of strong metal-support interaction (SMSI). *Applied Catalysis A: General 198*, 223-234. https://doi.org/10.1016/S0926-860X(99)00515-3.

Liu H., Liu C., Yin C., Liu B., Li X. and Li Y. (2016). Low temperature catalytic hydrogenation naphthalene to decalin over highly-loaded NiMo, NiW and NiMoW catalysts. *Catalysis Today 276*, 46-54. https://doi.org/10.1016/j.cattod.2016.03.024.

Lin S.D. and Vannice M.A. (1993). Hydrogenation of aromatic hydrocarbons over supported Pt catalysts. I. benzene hydrogenation. *Journal of Catalysis 143*, 539-573. https://doi.org/10.1006/jcat.1993.1297.

Luisetto I., Tuti S., Battocchio C., Lo S. and Sodo A. (2015). Ni/CeO_2-Al_2O_3 catalysts for the dry reforming of methane: The effect of $CeAlO_3$ content and nickel crystallite size on catalytic activity and coke resistance. *Applied Catalysis A 500*, 12-22. https://doi.org/10.1016/j.apcata.2015.05.004.

Liotta L.F. and Deganello G. (2003). Thermal stability, structural properties and catalytic activity of Pd catalysts supported on Al_2O_3-CeO_2-BaO mixed oxides prepared by sol-gel method. *Journal of Molecular Catalysis 204*, 763-770. https://doi.org/10.1016/S1381-1169(03)00362-5.

Mai H., Sun L., Zhang Y., Si R., Feng W., Zhang H., Liu H. and Yan Ch. (2005). Shape selective synthesis and oxygen storage behavior of ceria nanopolyhedra, nanorods, and nanocubes. *Journal of Physical Chemistry B 109*, 24380-24385. DOI: 10.1021/jp055584b.

Melchionna M. and Fornasiero, P. (2014). The role of ceria-based nanostructured materials in energy applications. *Materials Today 17*, 349-357. https://doi.org/10.1016/j.mattod.2014.05.005.

Morterra C. and Magnacca G. (1996). Surface characterization of modified aluminas. *Journal of the Chemical Society Faraday Transactions 92*, 1991-1996. http://dx.doi.org/10.1039/FT9969201991.

Profeti L.P.R., Ticianelli E.A., Assaf E.M. (2009). Production of hydrogen via steam reforming of biofuels on Ni/CeO_2-Al_2O_3 catalysts promoted by noble metals. *International Journal of Hydrogen Energy 34*, 5049-5274. https://doi.org/10.1016/j.ijhydene.2009.03.050.

Sánchez-Minero F., Ramírez J., Cuevas-García R. and Ríos-Castillo J. (2010). Hydrogenation of naphthalene using NiMo/Al_2O_3-$SiO_2(x)$ catalysts: Kinetic study. *Revista Mexicana de Ingeniería Química 9*, 151-158.

Sayle D, Maicaneanu, S. A. and Watson G. W. (2002). Atomistic models for CeO_2 (111), (110), and (100) nanoparticles, supported on yttrium-stabilized zirconia. *Journal of the American Chemical Society 124*, 11429-11439. DOI: 10.1021/ja020657f.

Téllez-Romero J.G., Cuevas-García R., Ramírez J. and Castillo-Villalón P. (2015). Simultaneous naphthalene and thiophene hydrogenation over Ni (X)-Pt/HMOR catalysts. *Catalysis Today 250*, 12-20. https://doi.org/10.1016/j.cattod.2014.08.032.

Torrente-Murciano L., Gilbank A., Puertolas B., Garcia T., Solsona B. and Chadwick D. (2013). Shape-dependency activity of nanostructured CeO_2 in the total oxidation of polycyclic aromatic hydrocarbons. *Applied Catalysis B: Environmental 132-133*, 116-122. https://doi.org/10.1016/j.apcatb.2012.10.030.

Tsivion D., Schvartzman, M., Popovitz-Biro R. and Joselevich E. (2012). Guided growth of horizontal zno nanowires with controlled orientations on flat and faceted sapphire surfaces. *Nanotechnology 6-7*, 6433-6445. DOI: 10.1021/nn3020695.

Venezia A.M., Parola V. La., Pawelec B. and Fierro J.L.G. (2004). Hydrogenation of aromatics over Au-Pd / SiO_2-Al_2O_3 catalysts?, support acidity effect. *Applied Catalysis A 264*, 43-51. https://doi.org/10.1016/j.apcata.2003.12.025.

Yuan Q., Duan, H., Li, L., Sun, L., Zhang, Y. and Yan Ch. (2009). Controlled synthesis and assembly of ceria-based nanomaterials. *Journal of Colloid Interface Science 335*, 151-167. https://doi.org/10.1016/j.jcis.2009.04.007.